Assessment of lignite upgrade and hydrogen evolution via electrolysis

Xiang Lyu [a,b]*, Junyi Hu [a,c]

[a] Chemical and Biomolecular Engineering Department

Ohio University

165 Stocker Center

Athens, OH 45701, USA

Phone: (1) 740-591-9596

e-mail: xl265816@ohio.edu

A research paper submitted to

Energy Conversion and Management

for consideration for publication

* Corresponding Author. E-mail address: xl265816@ohio.edu

[b] Electrification and Energy Infrastructures Division, Oak Ridge National Laboratory, Oak Ridge, TN 37831, USA

[c] University of Science and Technology Liaoning, School of Chemical Engineering, Key Laboratory of Functional Materials in Universities of Liaoning Province, Liaoning Anshan, 114051, P. R. China

ABSTRACT

lignite, considered as the lowest-rank coal, accounts for 45% of the total coal resources worldwide, and its low carbon and high ash contents limit its large-scale application. In order to upgrade lignite effectively, a modified coal electrolytic cell (MCEC) was designed, built, and then evaluated for lignite upgrade and hydrogen production through electrolysis, and the operating conditions were optimized. The results show that the performance of the MCEC outperformed our previous coal electrolytic cell (CEC). The operating temperature and iron concentration have a significant impact on the average current density per milligram of catalyst (ACDMC). The content of dry fixed carbon and heating value increased by 20.9% and 8.15%, respectively, in electrolyzed lignite compared with raw lignite. Besides. 71.5% ash and 39.6% mercury were removed from raw lignite after electrolysis, which is the first report. The Faradaic efficiency (FE) for hydrogen evolution reached 99.2% using MCEC. In addition, the analysis of spectroscopy methods (SEM, EDX, FTIR, and XRD) revealed that the lignite particles were cracked; the oxygen-containing functional groups increased; the minerals of quartz and hematite formed on the surface of lignite particles after electrolysis. The facts indicate that electrolysis of lignite is a competitive approach for lignite upgrade and hydrogen production.

Keywords: Lignite upgrade; Hydrogen evolution; Ash and mercury removal; Electrolysis

1. Introduction

Coal has been used as a solid fuel widely to produce electricity and heat by combustion through coal-fired power plants, from which more than 45% of electricity is generated in the USA [1]. Lignite, considered as the lowest-rank coal, accounts for about 45% of the total coal resources worldwide [2] and has a relatively low heat content due to its low carbon content and high ash content [3]. Burning this type of low-rank coal causes severe environmental issues due to contaminant and ash emissions [4]. Owing to the significant decrease of bituminous and anthracite coal [5-7], lignite will play a more critical role in coal-fired plants. Therefore, lignite upgrade is the first and necessary step to its further application, such as combustion, pyrolysis, and gasification [8-11]. Mineral matter is the inert solid material in the coal which forms ash during combustion [12]. It is challenging to reduce ash content to a minimum limit by physical method because the ash forming minerals are intermixed to the organic part of coal [13]. Thus, it is only possible to remove associated minerals via chemical methods. Behera et al. [13] investigated the chemical demineralization of high ash coal using alkali and acid solutions and found that 27% and 48% demineralization was achieved by treating coal using alkali and acid followed alkali, respectively. Liu et al. [14] evaluated the substantial upgrading of high-ash lignite by hydrothermal treatment followed by $Ca(OH)_2$ digestion/acid leaching. The results showed that the ash removal could reach 53.9% under operating conditions of alkali/ash mass ratio of 2 at 300 °C.

Moreover, mercury emission has attracted increasing attention in recent years because of its high toxicity, volatility, neurological health impact, and bioaccumulation in the environment [15, 16]. It is estimated that around one-third of the known anthropogenic mercury emissions in the United States [17], which can be attributed to coal combustion. Therefore, research on the

control of mercury emission from coal combustion is imperative. Post-combustion methods are currently the dominant approaches for managing mercury emission and can be classified into two main categories: Catalytic oxidation and sorbent injection [15]. Among these post-combustion methods for managing mercury emission, activated carbon injection has been proven to be one of the most promising technologies [18] and has been commercially deployed at coal-fired power plants for mercury capture since 2005 [19]. However, the remarkable disadvantages of activated carbon injection, including a high carbon to Hg ratio and adverse impacts on the commercial value of fly ashes, limit its application [20, 21]. Due to the negative aspects of post-combustion methods for controlling mercury emission, pre-combustion approaches for mercury removal are being developed. Unfortunately, only a few studies on the pre-combustion technologies for mercury removal (including physical, chemical, and thermal methods) from coal have been reported [22]. Consequently, it is important to find a pre-combustion approach for mercury removal that is cost-effective and eco-friendly.

Hydrogen is not only the most abundant element in the universe but also the cleanest fuel on the earth [23-25]. Besides, hydrogen has been considered a promising alternative to substitute conventional fossil fuels [26-29]. Currently, hydrogen is mainly produced from fossil fuels (reforming of natural gas, fractionation of petroleum, and gasification of coal) [30]. However, fossil fuels-based hydrogen production is non-renewable, and its byproducts are environmentally hazardous [31, 32]. In contrast to hydrogen production from fossil fuels, electrochemical water splitting for hydrogen evolution as an efficient and eco-environmental approach has attracted tremendous attention [33, 34]. However, water splitting also has some limitations, such as high energy consumption [35], low current efficiency [36], which limit its large-scale application.

Therefore, it is imperative to find an energy-efficient and environmentally friendly alternative for hydrogen production.

Coal electrolysis was first proposed by Coughlin and Farooque [37]. According to the authors, coal is oxidized at the anode based on the following reaction:

$$C + 2H2O \rightarrow CO_2 + 4H^+ + 4e^- \quad (1)$$

While protons are reduced to hydrogen at the cathode:

$$4H^+ + 4e^- \rightarrow 2H_2 \quad (2)$$

The standard theoretical potential for this process is just 0.21 V, which is significantly lower compared with the standard potential of water electrolysis at 1.23 V. Additionally, the actual energy consumption for hydrogen production through coal electrolysis is only one-third to one-half of the energy consumption via water electrolysis under similar operating conditions [38, 39]. It has been reported that the Faradaic efficiency of hydrogen via coal electrolysis could be close to 100% [37]. Due to the simplicity of the process (separation units are not required) and the low temperatures of the reaction, coal electrolysis for hydrogen production can find a potential market in distributed power and small hydrogen generators [40].

Though coal electrolysis seems to be a promising approach for hydrogen production, one of the problems associated with coal electrolysis is the low electro-oxidation rate of coal, making it economically unfavorable [40]. To overcome the issue, Patil et al. [40] evaluated the electro-oxidation rate of coal on different electrode materials and reported that Pt-Ir plated on Ti foil was the best electrode based on the current density. Sathe and Botte evaluated the coal electrolysis on carbon fiber electrodes plated with different noble metals Pt, Ir, and Rh. The authors found that the Pr-Ir outperformed all other electrodes with the same loading for converting coal to CO_2 [39].

Additionally, Jin and Botte performed coal electrolysis experiments on a coal electrolytic cell (CEC) using an anode of Pt-Ir plated on carbon fibers and stated that increasing temperature improved the kinetics of the coal electro-oxidation reaction, which significantly increased the conversion of coal to CO_2 [38].

Even though the electro-oxidation rate of coal can be enhanced by making electrodes with Pt-Ir catalyst, large quantities of noble metals are consumed in the process [38, 39]. The current density in coal electrolysis does not increase markedly in terms of per milligram of noble metal catalysts. Besides, plenty of sulfuric acid electrolytic solutions are consumed in the electrolysis process as well. Consequently, to make the process economically favorable, it is necessary to modify the CEC to minimize the use of noble metals and sulfuric acid electrolytic solutions and increase the electro-oxidation rate of coal.

To the best of our knowledge, there is no open literature about assessing lignite upgrade (through ash and mercury removal) and hydrogen production via electrolysis. With this content, this paper has three objectives as follows:

1.1. Modify the CEC reported by Jin and Botte [38] to a modified coal electrolytic cell (MCEC) to minimize noble metal catalyst loading and compare its performance with the CEC under similar operating conditions. Four operating conditions (lignite particle size, flow rate of lignite slurry, temperature, and iron concentration) were optimized based on the performance of the MCEC in terms of average current density per milligram of catalyst (ACDMC), indicating the electro-oxidation rate of coal. A factorial design was used to determine the effect of the four different operating conditions on the ACDMC, as this method can take into account interaction factors.

1.2. Determine the degree of ash removal from raw lignite through electrolysis under the optimal operating conditions obtained from the first objective. A blank experiment under optimal operating conditions without applied voltage was carried out as a comparison. Additionally, the changes of dry fixed carbon content and heating value in blank and electrolyzed lignite were analyzed and compared.

1.3. Evaluate the degree of mercury removal from raw lignite through electrolysis under the optimal operating conditions obtained from the first objective. The mercury removal condition in the blank experiment was investigated as well.

2. Material and methods

2.1. Synthesis of catalysts

Carbon-supported Pt and Pt-Ir catalysts were prepared via the polyol reduction method described in detail by Sheets and Botte [41]. Briefly, $H_2PtCl_6 \cdot 6H_2O$ (99.9% Purity, Purchased from Alfa Aesar) and $IrCl_3 \cdot 3H_2O$ (53-56% Ir, Purchased from Acros Organics) were used as metal precursors. 0.5 g of Carbon Vulcan XC-72 (100%, obtained from Cabot) was dispersed in a flask containing 200 ml of ethylene glycol (99% Purity, Purchased from Fisher Scientific) by agitation for 2 hours in a Branson 2800 Ultrasonic Bath, followed by the addition of a certain amount of metal precursors to achieve the desired 50 wt% loadings. The pH was balanced with 1 M KOH solution (Purchased from Fisher Scientific, certified 0.995-1.005 N). Then, the mixture was stirred with a magnetic stirring bar and refluxed at 175 °C for 16 h. After the reaction was completed, the catalyst was recovered using vacuum filtration with a polyamide membrane filter with a 0.2 μm pore size and washed with deionized (DI) water, followed by centrifuging for 45

minutes at 5000 rpm with a Centrifuge (Thermo Scientific Sorvall Legend X1 Centrifuge) and repeated two more times to remove the ethylene glycol completely. Finally, the obtained catalysts were dried at 110 °C under -0.08 MPa gauge pressure for 24 h to a constant weight.

2.2. Preparation of electrodes

According to Sathe and Botte [39], BASF Polyacrylonitrile (PAN) carbon fibers (from Celion G30-500, 7μm diameter) were still used for the anode preparation, as carbon fibers can provide a large surface for the electro-oxidation reactions. Hastelloy gauze (metal gauze 20 mesh gauze woven of 0.23 mm diameter wire from Alfa Aesar) was used as the current collector for the anode. Meanwhile, to increase the reaction contact area between the slurry and the anode, three pieces of Hastelloy gauzes wrapped with carbon fibers were used as the anode substrates. After the preparation of anode substrates, the catalysts of Pt-Ir were sprayed on the substrates with a loading amount of 1 mg cm^{-2}. In addition, in order to decrease the ohmic resistance between anode and cathode, the catalyst of Pt was sprayed on the nafion membrane (purchased from Sigma-Aldrich) directly with a loading amount of 0.1 mg cm^{-2}, which is used as the cathode. Besides, a piece of Hastelloy and a piece of carbon cloth were used as current collectors in the cathode, and the position of carbon cloth was between nafion membrane and Hastelloy gauze, in case of the destruction of nafion membrane caused by Hastelloy gauze. In addition, the electrodes were made in a circular shape with a diameter of 3 cm.

2.3. Construction of MCEC

Fig. 1 presented the schematic illustration of the MCEC, and the main constituents of the cell were anode and cathode compartments (A and G), the anode (Hastelloy wrapped with carbon fibers and catalyst) (B), O-ring (C), the cathode (nafion membrane with catalyst) (D), carbon

cloth (E), and Hastelloy mesh (F). The cell was made with Teflon rods (Virgin Electrical Grade Teflon rod with 76.2 mm diameter from McMaster-carr), which can withstand high operating temperature and sulfuric acid electrolyte. The anode and cathode compartments were separated by a nafion membrane. In order to minimize the use of sulfuric acid, the compartment of the cathode was kept empty without any electrolyte. The catalyst of Pt was sprayed on the nafion membrane in the cathode, resulting in decreasing the ohmic resistance and avoiding the abrasion of Pt catalyst.

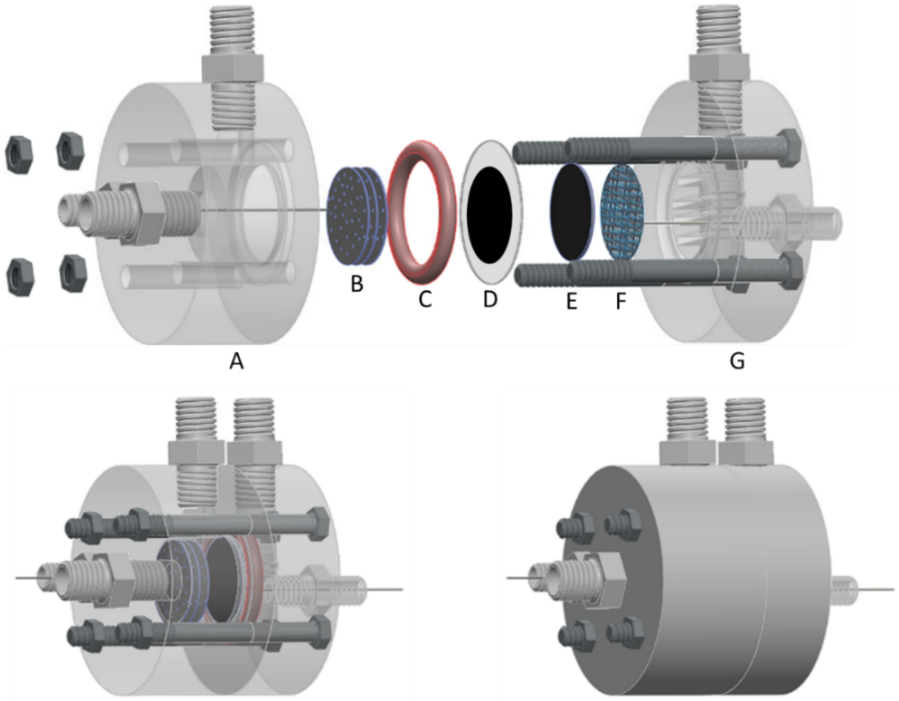

Fig. 1. Schematic illustration of the MCEC. The parts of the cell include: anode and cathode compartments (A and G), the anode of Hastelloy wrapped with carbon fibers and catalyst (B), O-ring (C), cathode of nafion membrane with catalyst (D), carbon cloth (E), and Hastelloy mesh (F).

In comparison with the CEC used by Jin and Botte [38], the MCEC has several advantages (see the ESI for the MCEC setup system): (1) three pieces of Hastelloy gauzes wrapped with carbon fibers used as anode substrates can increase the contact area between slurry and electrode surface to three times theoretically; (2) the nanoparticle Pt-Ir catalyst used at the anode can minimize the use of noble metal; (3) the catalyst of Pt sprayed on the nafion membrane directly in the cathode can decrease the ohmic resistance between anode and cathode obviously; (4) the absence of electrolyte in the cathodic compartment can save half of the sulfuric acid.

2.4. Characterization

The morphological characteristics of the raw, blank, and electrolyzed lignite samples were analyzed by scanning electron microscopy (SEM) using a JEOL-JSM- 639OLV operated at 15 K.V. The chemical compositions of the raw, blank, and electrolyzed lignite samples were determined by energy-dispersive X-ray (EDX) using a Genesis 2000-HX1622 attached to the SEM. The X-ray diffraction (XRD) patterns of the three lignite samples were collected on a Rigaku Ultima IV X-Ray Diffractometer with monochromatic Cu Kα radiation (λ=0.15405 nm) at a scanning rate of 2° min^{-1}. In addition, the infrared spectra of the three lignite samples were recorded in the 400-4000 cm^{-1} range by a Fourier transformed infrared spectrometer (Vertex 70/80 BRUKER) using KBr pellets. The proximate and mercury analysis of the three lignite samples were determined in Standard Laboratories, Inc. The gas composition was analyzed by gas chromatography (Agilent Technologies 7890B) with a packed column and thermal conductivity detector (TCD).

3. Results and discussion

3.1. Comparison of performance between MCEC and CEC

Fig. 2 showed the performance of MCEC and CEC. It can be seen that the ACDMC and AC of MCEC were 2.9 mA cm^{-1} per mg of catalyst and 60.9 mA, respectively. The ACDMC and the AC of CEC were only 0.22 mA cm^{-1} per mg of catalyst and 54.8 mA, respectively. The ACDMC of MCEC was 13.2 times higher than that of CEC, and the current density in MCEC was 1.11 times higher compared with CEC, indicating the performance of MCEC outperforms CEC. The possible reasons for the improvement are that the noble catalyst of Pt-Ir in MCEC is utilized more efficiently, and the ohmic resistance in MCEC is smaller than that in CEC.

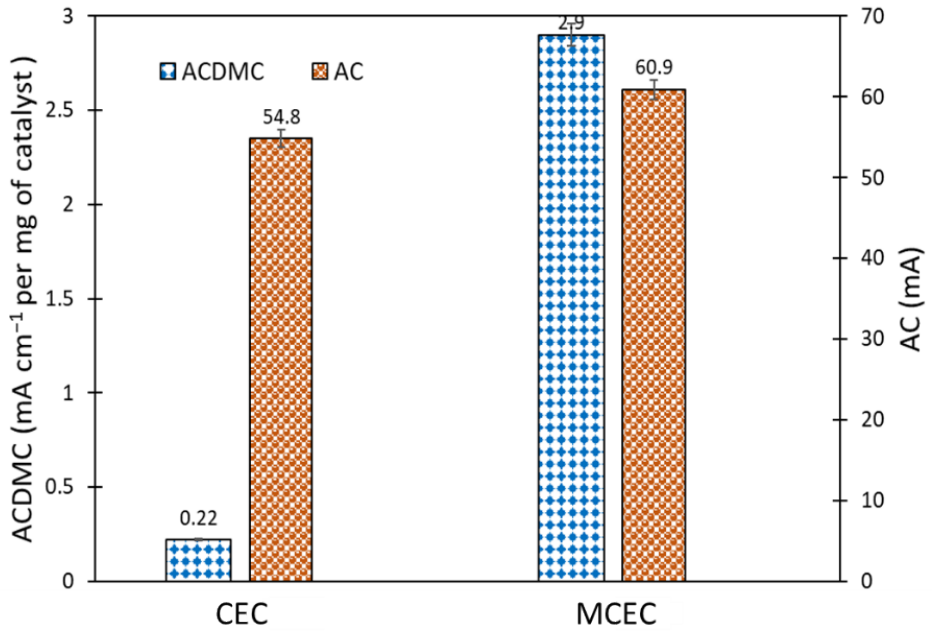

Fig. 2. The ACDMC and AC of CEC and MCEC. The ACDMC of MCEC is 13.2 times that of CEC, and the AC in MCEC is 1.11 times compared with CEC. The results show that the performance of MCEC outperforms CEC.

3.2. Evaluation of the performance of lignite electrolysis in long operating time (32 hours) under the optimal operating conditions

The optimal operating conditions for the electrolysis of lignite were obtained from the statistical analysis (see ESI for details). Fig. 3 showed the potentiostatic results for lignite electrolysis in a long working time (32 h) under the optimal operating conditions (small lignite particle: 105 µm, high flow rate: 300 ml min^{-1}, high temperature: 105 °C, and high iron concentration: 40 mM Fe (II) and Fe (III)).

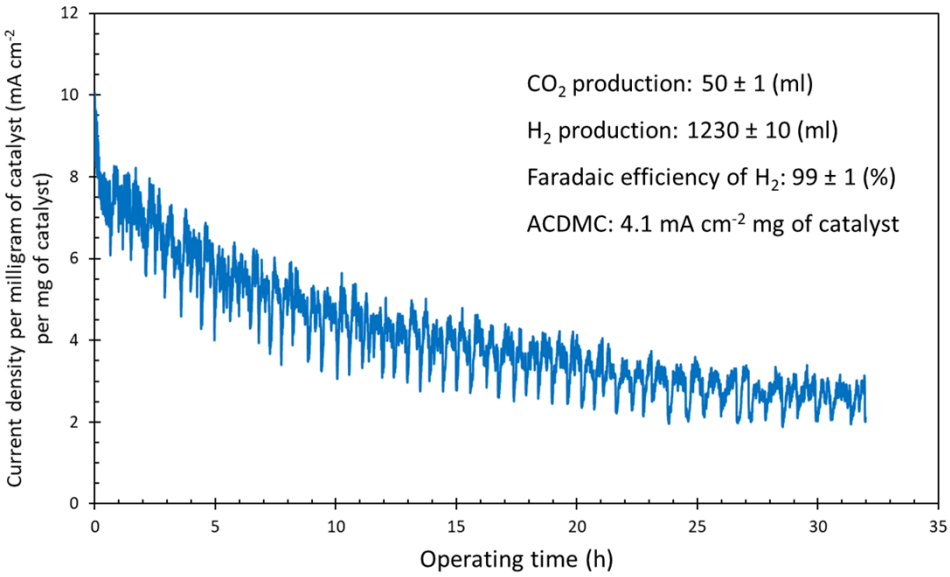

Fig. 3. Potentiostatic (1 V) results for lignite electrolysis under the optimal operating conditions (small lignite particle: 105 µm, high flow rate: 300 ml min-1, high temperature: 105 °C, and high iron concentration: 40 mM Fe (II) and Fe (III)). The results showed that the current density per milligram of catalyst decreased with the increase of operating time. The volume of H_2 production is 24.7 times that of CO_2, which indicates that the carbon in lignite is not oxidized completely. The Faradaic efficiency of hydrogen is almost 100%, as there is only a single reaction of proton reduction at the cathode.

It can be seen that the ACDMC decreased with the increase of operating time. The reason is that after the surface of coal is electro-oxidized, further electro-oxidation of coal is blocked by

the growth of films on the surface of the coal particles, as the films prevent the contact between the coal surface and electrode [42, 43]. Theoretically, the volume of H_2 should be two times compared with CO_2 production. Actually, the volume of H_2 is 24.7 times that of CO_2 based on the experimental results, which implies that the electro-oxidation of coal is not complete, and some intermediates are generated in the process. Moreover, the Faradaic efficiency of H_2 almost reaches 100%, as there is only a single reaction of proton reduction at the cathode. Meanwhile, the energy consumption for the hydrogen production through coal electrolysis was about 22.0 W h g^{-1}, which was 50 % lower than that for hydrogen production via water electrolysis under similar operating conditions [33].

3.3. Effect of electrolysis on dry fixed carbon content and dry heating value

Fig. 4(a) and (b) showed the dry fixed carbon content and dry heating value in raw, blank, and electrolyzed lignite samples, respectively. The raw, blank, and electrolyzed lignite samples were obtained from S1.3 (see ESI for details). It can be seen from Fig. 4(a) that the dry fixed carbon content in blank lignite increased by 16.1% compared with raw lignite (from 44.64% to 51.84%), and the dry fixed carbon in electrolyzed lignite was 20.9% higher than that of raw lignite, which suggests that the electrolysis is in favor of increasing dry fixed carbon content. There are two possible reasons for the increment of dry fixed carbon content in electrolyzed lignite, the ash removal and bond cleavage of C-COOH. The realease of formate and CO_2 from lignite during the electrolysis can increase the carobn content in the electrolyzed, as the carbon content in -COOH is only 26.7% (mass ratio). In comparison, there is only one possible reason for the increase of dry fixed carbon content in blank lignite, the ash removal, as some mineral matter in raw lignite can dissolve in sulfuric acid solution. Therefore, the increment of dry fixed carbon content in the electrolyzed lignite is higher than that of blank lignite. Besides, it can be seen from

Fig. 4(b) that the heating values in blank and electrolyzed lignite samples increased by 6.8% and 8.15% compared with raw lignite (from 23872 to 25498 and 25798 kJ/kg), respectively, and the reason for increasing heating values is the increment of dry fixed carbon content in blank and electrolyzed lignite samples. It should be noted that the increment of heating values is not precisely proportional to the increment of dry fixed carbon content in blank and electrolyzed lignite samples, as it is related to oxygen content as well.

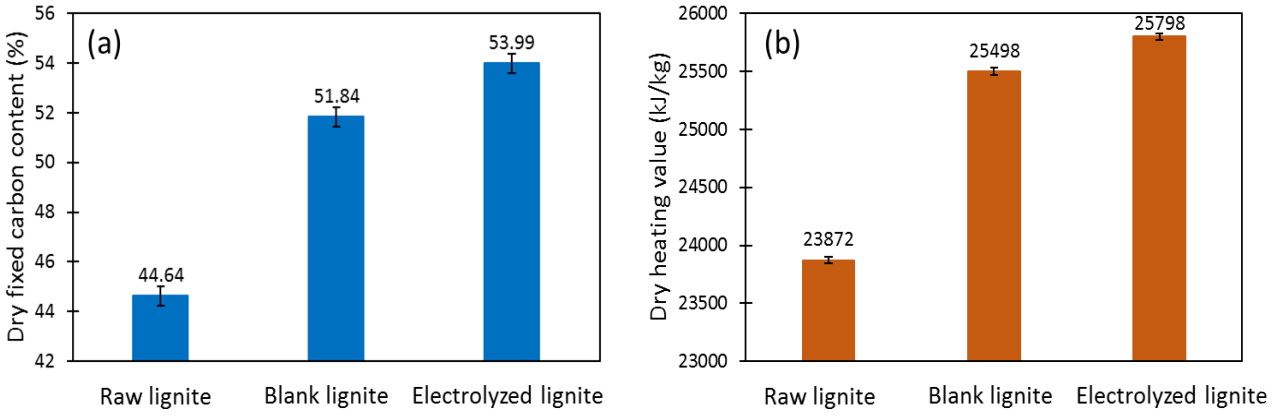

Fig. 4. Dry fixed carbon content (a) and dry heating value (b) in raw, blank, and electrolyzed lignite samples. The dry fixed carbon content and heating value in blank lignite are higher than that in raw lignite, and the electrolyzed lignite had the highest dry fixed carbon and heating value among the three samples.

3.4. Effect of electrolysis on dry ash content and mercury content

Fig. 5 (a) and (b) displayed the dry ash content and mercury content in raw, blank, and electrolyzed lignite samples, respectively. It can be seen from Fig. 5(a) that the ash contents in blank and electrolyzed lignite samples were just 29.1 and 28.5% compared with raw lignite (from 14.0 to 4.1 and 4.02%), respectively, which means 70.9 and 71.5% ashes are removed in blank and electrolyzed lignite samples, respectively. The results imply that the electrolysis does

not have much effect on ash removal from raw lignite, and the ash removal from raw lignite is mainly attributed to the effect of sulfuric acid solution. It can be seen from Fig. 5(b) that 26.4 and 39.6% mercury in blank and electrolyzed lignite samples were removed from raw lignite, which indicates that the electrolysis has a significant effect on mercury removal from lignite. The possible reason for mercury removal in the blank experiment is that some Hg^{2+} and Hg_p (Hg_p is formed when Hg^{2+} adsorbed to small particles) in raw lignite can dissolve into the sulfuric acid solution directly.

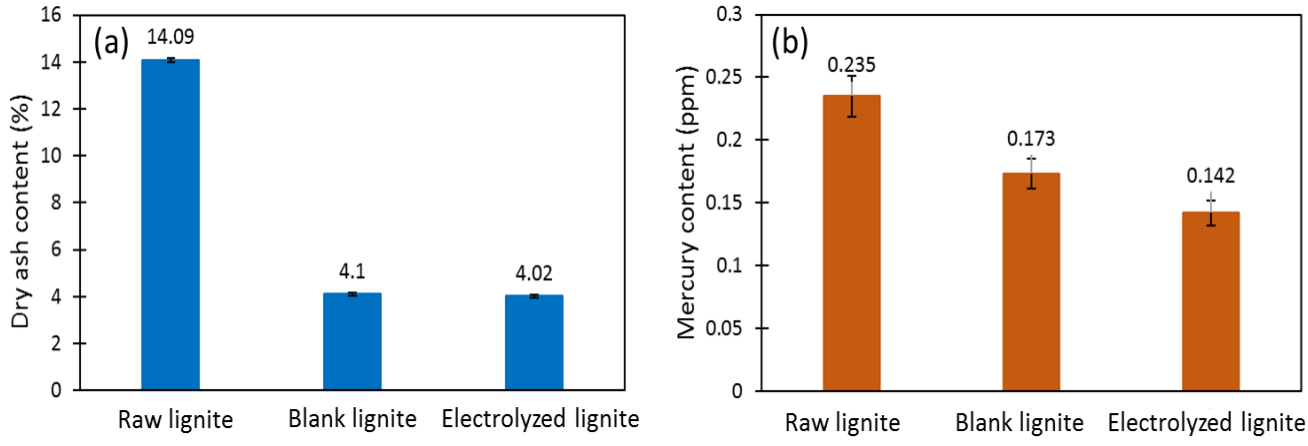

Fig. 5. Dry ash content (a) and mercury content (b) in raw, blank, and electrolyzed lignite samples. The dry ash content and mercury content in blank lignite were lower than raw lignite, and the electrolyzed lignite had the lowest dry ash content and mercury content among the three samples.

On the one hand, there are two possible reasons for mercury removal in electrolyzed lignite. One reason is the dissolving of Hg^{2+} and Hg_p into the sulfuric acid solution, and the other reason is that the Hg^0 is oxidized to Hg^{2+} by applying voltage and then dissolve into the electrolytic solution, as the standard potential of the oxidation of Hg^0 to Hg^{2+} is only 0.85 V versus SHE as shown in equation (3). Therefore, electrolysis affects mercury removal from raw lignite.

$$Hg^0 \rightarrow Hg^{2+} + 2e^- \quad (3)$$

3.5. SEM and EDX analysis of raw, blank, and electrolyzed lignite samples

The surface morphology of lignite samples was investigated by SEM. Fig. 6(a), (b), and (c) showed the SEM micrographs of raw, blank, and electrolyzed lignite samples, respectively. It can be seen that some structural changes occurred on the surface in blank and electrolyzed lignite samples, and the particle size of lignite becomes smaller in blank and electrolyzed lignite samples, especially in electrolyzed lignite sample, which indicates that cracks and exfoliation happened on the surface of electrolyzed lignite sample leading to the degradation. Besides, it can be seen clearly that the blank and electrolyzed lignite samples showed signs of agglomeration compared with raw lignite, and the electrolyzed lignite possessed a stronger intensity of agglomeration compared with the blank lignite.

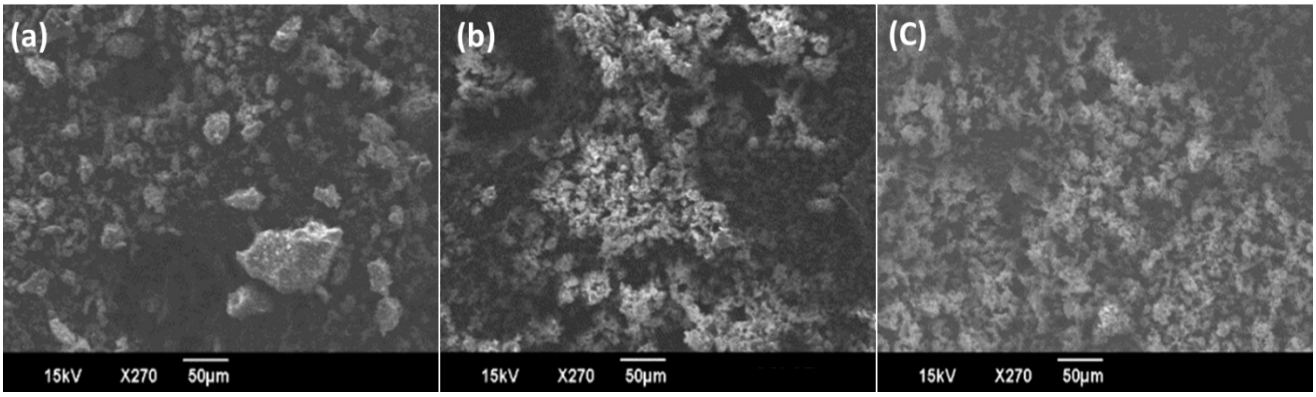

Fig. 6. SEM micrographs of lignite samples. (a) Raw lignite, (b) blank lignite, and (c) electrolyzed lignite. Blank and electrolyzed lignite samples all showed degradation and agglomeration compared with raw lignite, and the intensity of degradation and agglomeration in electrolyzed was higher than that of blank lignite.

Table 1 presents the EDX analysis corresponding to the SEM images of lignite samples. It can be seen that all the minerals (Mg, Al, Ca, and Ti) disappeared in blank and electrolyzed lignite samples, indicating the minerals are removed, which is consistent with the results from ash content analysis. In addition, it can be seen that Si content in blank lignite is 1.9 times compared with raw lignite (from 0.43% to 0.83%), the possible reasons for the increment are that Si does not dissolve into the sulfuric acid solution, and more and more Si is exposed with the crack of lignite and the removal of other minerals. Meanwhile, the Si content in electrolyzed lignite sample is 4.02 times that of raw lignite, implying that the particle size of lignite is cracked to a smaller size and more Si is exposed compared with blank lignite, and the results are in agreement with the results from SEM analysis. Moreover, the C content decreased by 4.9%, and the O content increased by 28% on the surface of electrolyzed lignite. In contrast, the C and O contents just changed slightly in blank lignite compared with raw lignite, which suggests some carbon is electro-oxidized on the lignite surface. The electro-oxidation of carbon is not complete, and the results are in agreement with Section 3.2. It should be noted that the mercury was not observed by EDX, as the mercury content is too low.

Table 1

EDX analysis corresponding to the SEM images of lignite samples.

Elements / Samples	C (At%)	O (At%)	Si (At%)	S (At%)	Mg (At%)	Al (At%)	Ca (At%)	Ti (At%)
Raw lignite	82 ±1	16 ±1	0.4 ± 0.1	0.3 ± 0.1	0.2 ± 0.1	0.5 ± 0.1	0.8 ± 0.1	0.2 ± 0.1
Blank lignite	82 ±1	17 ±1	0.8 ± 0.1	0.5 ± 0.1	0	0	0	0
Electrolyzed lignite	78 ±1	20 ±1	1.7 ± 0.1	0.4 ± 0.1	0	0	0	0

3.6. FTIR analysis of raw, blank, and electrolyzed lignite samples

FTIR spectra of raw, blank, and electrolyzed lignite samples were shown in Fig. 7. According to Fig. 7(a), the notable difference between raw lignite and the other two lignite samples was

between the wavenumber of 1800 and 900 cm^{-1}, so the range from 1800 to 900 cm^{-1} was presented as Fig. 7(b). It can be seen that a new peak around 1700 cm^{-1} appeared in blank and electrolyzed lignite samples compared with raw lignite, and the intensity of the peak at 1700 cm^{-1} in electrolyzed lignite is significantly stronger than that of blank lignite. In addition, the peaks at 1700 and 1620 cm^{-1} are attributed to the carboxyl group (-COOH) [44], and the intensity of the peak at 1450 cm^{-1} related to carbonates [45] increased in electrolyzed lignite when compare to raw lignite. Meanwhile, another new band in the range from 1300 to 1100 cm^{-1} appeared in electrolyzed lignite, which is assigned to the C-O-C and C-O-H vibrations [46, 47]. The results showed that the oxygen-containing functional groups increase on the surface of electrolyzed lignite compared with blank and raw lignite samples, which are consistent with the EDX analysis. Moreover, the results reveal why the production of CO_2 volume is significantly less than the H_2 volume, as the electro-oxidation of lignite is not complete.

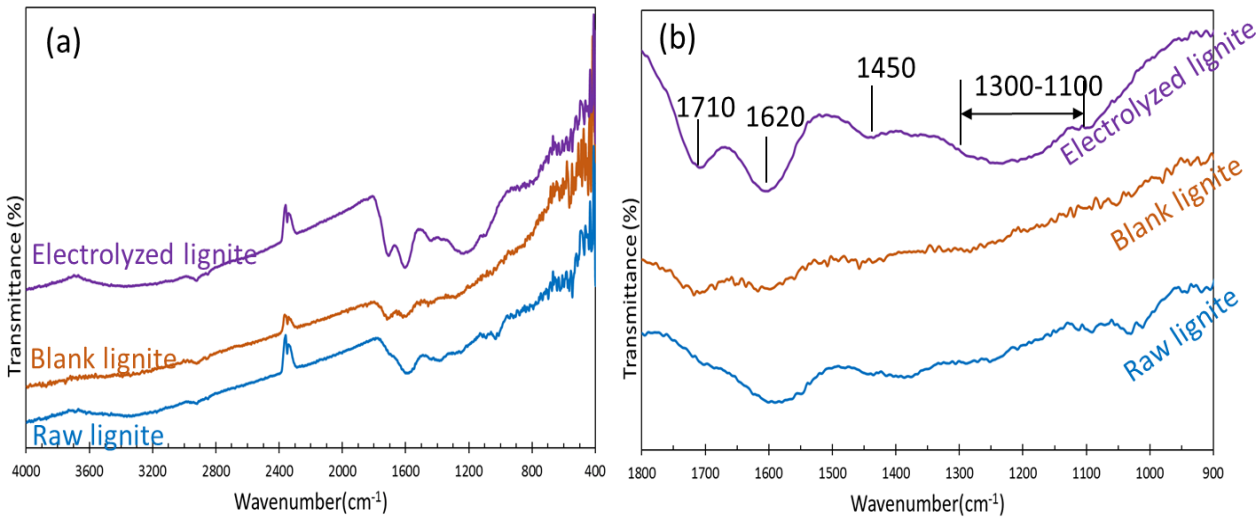

Fig. 7. FTIR spectra of raw, blank, and electrolyzed lignite samples. (a) Range from 4000 to 400 cm^{-1}, and (b) range from 1800 to 900 cm^{-1}. The notable differences between raw lignite and the other two lignite samples were between the wavenumber of 1800 and 900 cm^{-1}. The peaks at 1700 and 1620 cm^{-1} are attributed to the carboxyl group (-COOH). The peak at 1450 cm^{-1} can be attributed to the carbonates, and the peak between 1300 to 1100 cm^{-1} is assigned to the C-O-C

and C-O-H vibrations. The results suggested that the oxygen-containing functional groups increase in electrolyzed lignite compared with blank and raw lignite samples.

3.7. XRD analysis of raw, blank, and electrolyzed lignite samples

XRD spectrum of raw, blank, and electrolyzed lignite samples were shown in Fig. 8. The major minerals are identified as the following: Kaolinite (K), magnetite (M), quartz (Q), hematite (H), pyrite (P), and siderite (S) [5, 42, 44, 48]. Notable differences were observed between raw lignite and the other two lignite samples, and there was no apparent difference between blank and electrolyzed lignite samples. The intensity of the peaks corresponding to kaolinite (12°, 25°, and 60°) almost disappeared in blank and electrolyzed lignite samples compared with raw lignite, while the intensity of peaks corresponding to quartz (26.5°) and hematite (36°) increased in electrolyzed lignite when compared to raw and blank lignite samples. In addition, the intensity of peaks attributed to magnetite (43°), pyrite (33°), and siderite (31.5°) almost kept constant among the three lignite samples. According to the XRD analysis, it could be hypothesized that the formation of quartz and hematite on the surface of lignite particles is one reason for the deactivation of lignite during electrolysis.

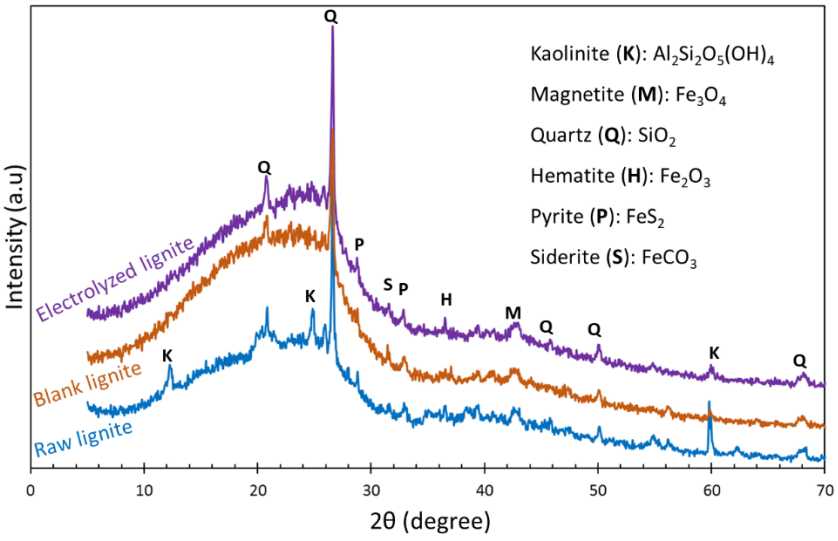

Fig. 8. XRD spectra of raw, blank, and electrolyzed lignite samples. The following minerals were identified: Kaolinite (K), magnetite (M), quartz (Q), hematite (H), pyrite (P), and siderite (S).

4. Conclusion

Hydrogen production and lignite upgrade were investigated on the MCEC via electrolysis. The experimental results showed that the ACDMC in MCEC was 13.2 times that in CEC, indicating that the performance of MCEC was much superior to the CEC. According to the statistical analysis, the iron concentration and operating temperature had a significant effect on ACDMC. In addition, the Faradaic efficiency of hydrogen could reach 99% in a long operating time (32 h). The content of dry fixed carbon increased by 20.9%, and the heating value increased by 8.15% in electrolyzed lignite compared with raw lignite. Moreover. 71.5% ash and 39.6% mercury were removed in electrolyzed lignite when compared to raw lignite. SEM and EDX revealed that the lignite particles were cracked, and the oxygen content increases on the surface of lignite particles. The FTIR analysis implied that the oxygen-containing functional groups increased in electrolyzed lignite, and the electro-oxidation of lignite was not complete, which was in agreement with the results from EDX. Additionally, XRD analysis suggested that the formation of quartz and hematite on the surface of lignite particles might be one reason for the deactivation of lignite during electrolysis. The facts demonstrate that electrolysis is a promising method for hydrogen production and lignite upgrade.

Acknowledgments

The authors would like to acknowledge the financial support of the Center for Electrochemical Engineering Research at Ohio University and the Ishikawajima-Harima Heavy Industries Co., Ltd. (IHI).

References

[1] T.M. Gur. Critical Review of Carbon Conversion in "Carbon Fuel Cells". Chemical Reviews. 113 (2013) 6179-206.
[2] Q.S. Li, Y.K. Lin. Exergy analysis of the LFC process. Energy Conversion and Management. 108 (2016) 348-54.
[3] L.Y. Liu, W.D. Chen, Y.Q. Li. An overview of the proton conductivity of nafion membranes through a statistical analysis. Journal of Membrane Science. 504 (2016) 1-9.
[4] Z. Zhang, C.M. Liu, W. Liu, Y. Cui, X. Du, D. Xu, et al. Innovative design of coal utilization - A green pathway for direct conversion of coal to electricity through flow fuel cell technology. Applied Energy. 200 (2017) 226-36.
[5] L. Ding, Y. Gong, Y.F. Wang, F.C. Wang, G.S. Yu. Characterisation of the morphological changes and interactions in char, slag and ash during CO2 gasification of rice straw and lignite. Applied Energy. 195 (2017) 713-24.
[6] G.F. Chen, X.F. Yang, S.Y. Chen, Y. Dong, L. Cui, Y. Zhang, et al. Transformation of heavy metals in lignite during supercritical water gasification. Applied Energy. 187 (2017) 272-80.
[7] X. Zhu, S. Li, Z. Luo, X. Zhu. Combined with fractional condensation to upgrade the liquid products derived from the co-pyrolysis of bio-oil distillation residue and bituminous coal. Energy Conversion and Management. 185 (2019) 586-92.
[8] H.J. Li, Q.H. Chang, R. Gao, Z.H. Dai, X.L. Chen, G.S. Yu, et al. Thin-layer drying characteristics and modeling of lignite under supercritical carbon dioxide extraction and the evolution of pore structure and reactivity. Fuel Processing Technology. 170 (2018) 1-12.
[9] H.J. Li, Q.H. Chang, R. Gao, Z.H. Dai, X.L. Chen, G.S. Yu, et al. Fractal characteristics and reactivity evolution of lignite during the upgrading process by supercritical CO2 extraction. Applied Energy. 225 (2018) 559-69.
[10] L. Lu, Y. Fang, Z. Huang, Y. Huang, Z.J. Ren. Self-sustaining carbon capture and mineralization via electrolytic carbonation of coal fly ash. Chemical Engineering Journal. 306 (2016) 330-5.
[11] Q. He, L. Ding, A. Raheem, Q. Guo, Y. Gong, G. Yu. Kinetics comparison and insight into structure-performance correlation for leached biochar gasification. Chemical Engineering Journal. 417 (2021) 129331.
[12] J. Wang, Z.G. Zhang, Y. Kobayashi, A. Tomita. Chemistry of Ca(OH)(2) leaching on mineral matter removal from coal. Energy & Fuels. 10 (1996) 386-91.
[13] S.K. Behera, S. Chakraborty, B.C. Meikap. Chemical demineralization of high ash Indian coal by using alkali and acid solutions. Fuel. 196 (2017) 102-9.
[14] X.P. Liu, X.T. Wu, J. Wang. Substantial upgrading of a high-ash lignite by hydrothermal treatment followed by Ca(OH)(2) digestion/acid leaching. Fuel. 222 (2018) 269-77.
[15] H.T. Zhao, X.L. Mu, G. Yang, M. George, P. Cao, B. Fanady, et al. Graphene-like MoS2 containing adsorbents for Hg-0 capture at coal-fired power plants. Applied Energy. 207 (2017) 254-64.

[16] S. Liang, Y.F. Wang, S. Cinnirella, N. Pirrone. Atmospheric Mercury Footprints of Nations. Environmental Science & Technology. 49 (2015) 3566-74.
[17] A.A. Presto, E.J. Granite. Survey of catalysts for oxidation of mercury in flue gas. Environmental Science & Technology. 40 (2006) 5601-9.
[18] H.Q. Yang, Z.H. Xu, M.H. Fan, A.E. Bland, R.R. Judkins. Adsorbents for capturing mercury in coal-fired boiler flue gas. Journal of Hazardous Materials. 146 (2007) 1-11.
[19] S. Sjostrom, M. Durham, C.J. Bustard, C. Martin. Activated carbon injection for mercury control: Overview. Fuel. 89 (2010) 1320-2.
[20] Y. Liu, D.J.A. Kelly, H.Q. Yang, C.C.H. Lin, S.M. Kuznicki, Z.G. Xu. Novel regenerable sorbent for mercury capture from flue gases of coal-fired power plant. Environmental Science & Technology. 42 (2008) 6205-10.
[21] L. Zhang, Y.Q. Zhuo, W. Du, Y. Tao, C.H. Chen, X.C. Xu. Hg Removal Characteristics of Noncarbon Sorbents in a Fixed-Bed Reactor. Industrial & Engineering Chemistry Research. 51 (2012) 5292-8.
[22] G.Q. Luo, J.J. Ma, J. Han, H. Yao, M.H. Xu, C. Zhang, et al. Hg occurrence in coal and its removal before coal utilization. Fuel. 104 (2013) 70-6.
[23] J.A. Turner. Sustainable hydrogen production. Science. 305 (2004) 972-4.
[24] M.I. Hoffert, K. Caldeira, G. Benford, D.R. Criswell, C. Green, H. Herzog, et al. Advanced technology paths to global climate stability: Energy for a greenhouse planet. Science. 298 (2002) 981-7.
[25] G. Kakoulaki, I. Kougias, N. Taylor, F. Dolci, J. Moya, A. Jäger-Waldau. Green hydrogen in Europe–A regional assessment: Substituting existing production with electrolysis powered by renewables. Energy Conversion and Management. 228 (2021) 113649.
[26] Y. Jiao, Y. Zheng, M.T. Jaroniec, S.Z. Qiao. Design of electrocatalysts for oxygen- and hydrogen-involving energy conversion reactions. Chemical Society Reviews. 44 (2015) 2060-86.
[27] M. Aasadnia, M. Mehrpooya. Large-scale liquid hydrogen production methods and approaches: A review. Applied Energy. 212 (2018) 57-83.
[28] P. Guo, Z. Xiong, S. Yuan, K. Xie, H. Wang, Y. Gao. The synergistic effect of Co/CoO hybrid structure combined with biomass materials promotes photocatalytic hydrogen evolution. Chemical Engineering Journal. (2021) 130372.
[29] K. Xie, P. Guo, Z. Xiong, S. Sun, H. Wang, Y. Gao. Ni/NiO hybrid nanostructure supported on biomass carbon for visible-light photocatalytic hydrogen evolution. Journal of Materials Science. 56 (2021) 12775-88.
[30] M. Kokko, F. Bayerkohler, J. Erben, R. Zengerle, P. Kurz, S. Kerzenmacher. Molybdenum sulphides on carbon supports as electrocatalysts for hydrogen evolution in acidic industrial wastewater. Applied Energy. 190 (2017) 1221-33.
[31] A. Heinzel, B. Vogel, P. Hubner. Reforming of natural gas - hydrogen generation for small scale stationary fuel cell systems. Journal of Power Sources. 105 (2002) 202-7.
[32] G.J. Stiegel, M. Ramezan. Hydrogen from coal gasification: An economical pathway to a sustainable energy future. International Journal of Coal Geology. 65 (2006) 173-90.
[33] J. Li, A. Listwan, J. Liang, F. Shi, K. Li, J. Jia. High proportion of 1 T phase MoS2 prepared by a simple solvothermal method for high-efficiency electrocatalytic hydrogen evolution. Chemical Engineering Journal. 422 (2021) 130100.
[34] J. Xu, S. Wang, C. Yang, T. Li, Q. Liu, X. Kong. Free-standing two-dimensional ruthenium-beryllium nanosheets for alkaline hydrogen evolution. Chemical Engineering Journal. 421 (2021) 129741.
[35] K. Zeng, D.K. Zhang. Recent progress in alkaline water electrolysis for hydrogen production and applications. Progress in Energy and Combustion Science. 36 (2010) 307-26.
[36] C. Yilmaz, M. Kanoglu. Thermodynamic evaluation of geothermal energy powered hydrogen production by PEM water electrolysis. Energy. 69 (2014) 592-602.

[37] R.W. Coughlin, M. Farooque. HYDROGEN PRODUCTION FROM COAL, WATER AND ELECTRONS. Nature. 279 (1979) 301-3.
[38] X. Jin, G.G. Botte. Feasibility of hydrogen production from coal electrolysis at intermediate temperatures. Journal of Power Sources. 171 (2007) 826-34.
[39] N. Sathe, G.G. Botte. Assessment of coal and graphite electrolysis on carbon fiber electrodes. Journal of Power Sources. 161 (2006) 513-23.
[40] P. Patil, Y. De Abreu, G.G. Botte. Electrooxidation of coal slurries on different electrode materials. Journal of Power Sources. 158 (2006) 368-77.
[41] B.L. Sheets, G.G. Botte. Electrochemical nitrogen reduction to ammonia under mild conditions enabled by a polymer gel electrolyte. Chemical Communications. 54 (2018) 4250-3.
[42] Y. De Abreu, P. Patil, A.I. Marquez, G.G. Botte. Characterization of electrooxidized Pittsburgh No. 8 Coal. Fuel. 86 (2007) 573-84.
[43] X. Jin, G.G. Botte. Understanding the kinetics of coal electrolysis at intermediate temperatures. Journal of Power Sources. 195 (2010) 4935-42.
[44] X.Z. Gong, M.Y. Wang, Z. Wang, Z.C. Guo. Desulfuration of electrolyzed coal water slurry in HCl system with ionic liquid addition. Fuel Processing Technology. 99 (2012) 6-12.
[45] H. Zareie, N. Oztas, M. Gundogan, E. Piskin, Y. Yurum. Images of demineralized coal surfaces by scanning tunnelling microscopy. Fuel. 75 (1996) 855-7.
[46] T.M. Cui, W.K. Fan, Z.H. Dai, Q.H. Guo, G.S. Yu, F.C. Wang. Variation of the coal chemical structure and determination of the char molecular size at the early stage of rapid pyrolysis. Applied Energy. 179 (2016) 650-9.
[47] M. Baysal, A. Yurum, B. Yildiz, Y. Yurum. Structure of some western Anatolia coals investigated by FTIR, Raman, C-13 solid state NMR spectroscopy and X-ray diffraction. International Journal of Coal Geology. 163 (2016) 166-76.
[48] X.C. Lin, M. Luo, S.Y. Li, Y.P. Yang, X.J. Chen, B. Tian, et al. The evolutionary route of coal matrix during integrated cascade pyrolysis of a typical low-rank coal. Applied Energy. 199 (2017) 335-46.